# Hydrothermal Synthesis of Ultra-high Aspect Ratio β-NaYF Disks via Methyliminodiacetic Acid (MIDA)

Lars Forberger<sup>1</sup>, Jacob T. Baillie<sup>2</sup>, Zhaojie Feng<sup>1</sup>, Rachel E. Gariepy<sup>1</sup>, Sankhya Hirani<sup>1</sup>, Daniel R. Gamelin<sup>2</sup>, Shuai Zhang<sup>1, 3</sup>, Werner Kaminsky<sup>2</sup>, and Peter J. Pauzauskie<sup>\*1, 4</sup>

<sup>1</sup>Department of Materials Science & Engineering, University of Washington, Seattle, WA 98195, USA

<sup>2</sup>Department of Chemistry, University of Washington, Seattle, WA 98195, USA
 <sup>3</sup>Physical Sciences Division, Pacific Northwest National Laboratory, Richland, WA 99354, USA

<sup>4</sup>Physical and Computational Sciences Directorate, Pacific Northwest National Laboratory, Richland, WA 99354, USA

\*Email Address: peterpz@uw.edu

November 20, 2025

#### Abstract

The hexagonal β-phase of sodium yttrium fluoride (NaYF) is a leading host material for lanthanide upconversion and anti-Stokes fluorescence laser refrigeration based on its low phonon energies and high upconversion efficiency. Recently experiments have been proposed to use this material as an optically-levitated sensor of high-frequency gravitational waves. In order to maximize signal-to-noise in this experiment, the NaYF sensor must have both a two-dimensional, disk-like morphology and also a large mass. Here we report a novel hydrothermal process based on the chelation ligand methylimidodiacetic acid (MIDA) to realize hexagonal  $\beta$ -NaYF prisms with corner-to-corner diameters up to 44 µm while keeping the height around 1 µm. The surface quality is comparable to particles synthesized with EDTA based on atomic force microscopy (AFM) measurements. Unlike particles synthesized with EDTA the  $\beta$ -NaYF particles show no lensing based on curvature of the hexagonal basal plane. Single crystal X-ray diffraction data were refined to the  $P\bar{6}2c$  (#190) space group which to the best of our knowledge has not been reported in the literature. One of six 44 μm β-NaYF disks doped with 10 % ytterbium showed laser refrigeration of  $(-4.9\pm1.0)$  K suggesting future applications in both levitated optomechanics and microoptics.

#### 1 Introduction

Upconversion materials are widely studied for potential applications such as physical sensors, biosensors, artificial light sources, displays, anti-counterfeiting agents and solar cell enhancers [1, 2, 3, 4, 5, 6]. The materials developed for most of these applications are on the nanoscale and doped with combinations of lanthanides to achieve visible output following nearinfrared (NIR) excitation based on multiphoton upconversion. Microparticles are less suitable for some of the aforementioned applications but are more relevant in microoptics, e.g. as microlaser cavities [7, 8, 9]. Using ytterbium (Yb<sup>3+</sup>) as a dopant furthermore adds the possibility of anti-Stokes fluorescence laser refrigeration offering additional hypothetical uses like temperature controlled micromirrors, microlenses, waveguides, radiation balanced lasers, and payload cooling substrates [10, 11]. Levitated-sensor applications benefit from laser refrigeration as well due to the avoidance of the negative effects associated with heating, like thermal noise, motional instability, and sample degradation. Examples include high-precision accelerometers and the detection of high frequency gravitational waves using high-mass sensors optically levitated in two arms of a Michelson interferometer [12]. Many of these systems require specific particle morphologies, sizes, and masses in order to trap the sensors, reach sensitivity goals or generate the desired motional dynamics[13]. Here, we focus on the design of high-mass hexagonal disks that can be trapped in the antinode of a dual-beam standing wave trap, limiting the particle thickness to roughly 1 µm. To increase the mass of the particles, we aim to maximize the corner-to-corner diameter and accordingly diameter-to-thickness aspect ratio (AR), while maintaining the laser refrigeration capabilities made possible through ytterbium (Yb<sup>3+</sup>) doping. The cooling and disk-like morphology enhance the readout quality by reducing the thermal noise and maximizing light scattering in the forward direction where detection occurs [12, 13].

Since its original discovery [14, 15], the hexagonal  $\beta$ -phase of sodium yttrium fluoride ( $\beta$ -NaYF) has been demonstrated to be one of the most efficient upconversion host materials and has been studied extensively [16]. Single crystals of  $\beta$ -NaYF can be synthesized via multiple different routes, including melt growth, thermal decomposition, coprecipitation and solvo- or hydrothermal methods [17, 18, 4]. Melt growth approaches to obtain macroscopic samples have failed in the past [17, 18], resulting in upper size limits of single crystalline par-

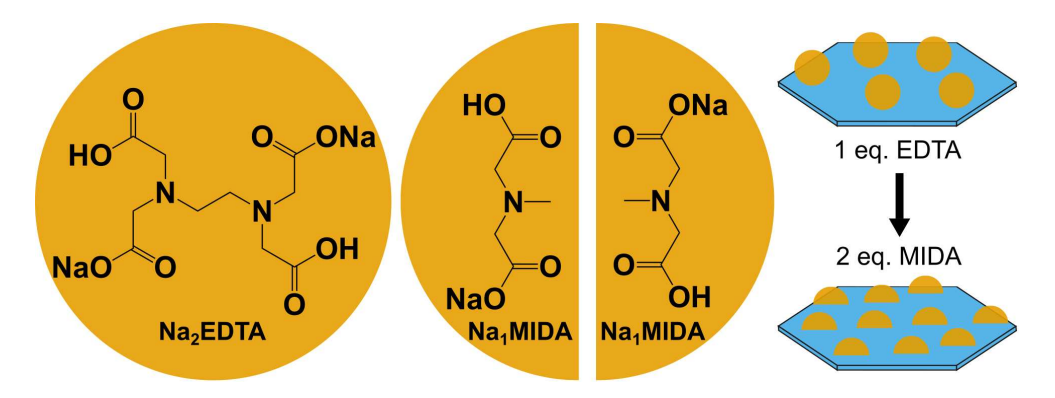


Figure 1: Chemical structures of EDTA and MIDA. Illustration of the hypothetical surface coverage increase on a  $\beta$ -NaYF nucleus by substituting EDTA with two equivalents of MIDA.

ticles in the micron range. These are most commonly obtained using hydrothermal synthesis, where the size and morphology are controlled by the addition of organic molecules. These often have a twofold functionality, acting as chelating agents as well as surface adsorbents that alter the nucleation and growth thermodynamics and kinetics. The most commonly used organic additives are sodium citrate and ethylenediaminetetraacetic acid (EDTA). We are unaware of synthesis optimizations towards hexagonal disks and the typical diameter obtained is to the best of our knowledge below 5  $\mu$ m [19, 20, 21, 22, 23, 24, 25, 26, 27, 28, 29, 30]. Felsted et al. showed that EDTA can be used to tune the morphology of  $\beta$ -NaYF fluently from hexagonal plates to rods by changing the ratio of rare-earth (RE) to fluoride ions. The largest hexagonal disk obtained had a diameter of 5  $\mu$ m and  $\sim$ 500 nm heights, resulting in an aspect ratio of 10.5 [31].

The fundamental idea of this work is to increase the surface coverage of ligands during growth by substituting one molecule of EDTA with two molecules of methyliminodiacetic acid (MIDA). MIDA is effectively half an EDTA molecule, and two equivalents should in principle be able to yield a comparable control over the particle morphology. While the RE-MIDA complex will be less stable than the RE-EDTA equivalent for entropic reasons [32], the surface coverage on a flat surface should be increased, as illustrated in Figure 1. Furthermore, MIDA has a higher solubility than EDTA allowing a wider range of pH values to be explored within the available thermodynamic parameter space. Both EDTA and MIDA exist in different ionic species depending on the pH of the solution due to the acidic carboxylic acid and basic amine groups as shown for MIDA in Figure 2. Here, the pH-dependent morphology control of β-NaYF during the MIDA-assisted hydrothermal synthesis is presented. At pH values below the inflection point, rods are obtained. Increasing the amount of NaOH to 1 eq. yields hexagonal disks with corner-to-corner width up to 44 µm. Beyond the inflection point, semicircular disks were observed before hexagonal prisms were obtained in the high-pH regime. Single crystal Xray diffraction of individual  $Na_{1.00}MIDA$   $\beta$ -NaYF disk indicate they have a  $P\bar{6}2c$  space group that, to the best of our knowledge, has not yet been reported. Further, one of six measured particles showed laser refrigeration of  $(-4.9 \pm 1.0)$  K opening avenues towards future solidstate laser refrigeration of these microdiscs within both optically-levitated gravitational wave interferometers and integrated optoelectronic devices.

#### 2 Results and Discussion

The influence of MIDA as an organic additive on the size and morphology of hydrothermally grown  $\beta$ -NaYF was investigated and compared to EDTA. During the optimization, aiming for high aspect ratio disks with heights below 1 µm, different protonation states of MIDA were studied by dissolving the ligand with different amounts of sodium hydroxide (NaOH) ranging from 0 eq. to 2 eq. Since the MIDA titration curve has an inflection point at 1 eq. NaOH with a predicted pH value of 6.12, as shown in Figure 2, two syntheses with pH values just above and below the inflection point were run. The amount of NaOH used heavily affects the phase distribution, size and morphology of the product as shown in **Table 1**. Powder X-ray diffraction (XRD) was used to determine the synthesized phase(s) and scanning electron microscopy (SEM) was used to assess the particle morphology and size. While  $\beta$ -NaYF is obtained under all conditions, the addition of low amounts of NaOH ( $\leq$  0.50 eq.) led to the formation of yttrium trifluoride (YF<sub>3</sub>) as byproduct. The syntheses using 0.75 eq. to 1.50 eq. resulted in mixed  $\alpha$ - and  $\beta$ -phases with the exception of Na<sub>1.00</sub>MIDA above the pH inflection

point. The α-NaYF particles were sub 100 nm spheres, very comparable to those obtained in hydrothermal synthesis at lower temperatures, typically 90 °C using EDTA and otherwise similar conditions [33]. 2.00 eq. NaOH was the only amount consistently yielding phase-pure  $\beta$ -NaYF. Due to the large mass difference between the  $\beta$ -NaYF microparticles and  $\alpha$ -NaYF nanoparticles a simple separation by supernatant removal from EtOH dispersions was used to obtain the hexagonal disks prior to any further characterization (see Figure S1). From the lowest to highest amount of added NaOH the β-NaYF particle morphology changed from rods to hexagonal disks to semicircular disks and eventually back to hexagonal disks (see Figure 2 and S2). It is noteworthy that the organic redsidue appearing black in the SEM images is from the EtOH used for dropcasting and not a synthesis residue as illustrated in Figure S3. The prisms obtained with 2.00 eq. of NaOH appear to be several fused hexagonal disks (Figure S2 (d)) while the particles obtained at 1.00 eq. show very clear hexagonal faceting without any obvious defects visible in SEM or optical microscope images (Figure 2 ((d), (f) and (f)). The optical microscopy images further illustrate the transparency of  $\beta$ -NaYF in the visible spectrum and point towards applications as microoptics. From 0.00 eq. to 0.75 eq. NaOH the hexagonal rods were obtained. The width increased from 3.4 µm for the first two amounts to 8.7 μm, and the length from 15.6 μm over 16.8 μm to 42.1 μm (Table 1, Figure 2 (c) and Figure S2 (a), (b)) resulting in a width-to-height aspect ratio (AR) of roughly 0.2 for all rod-like morphologies. The hexagonal disks obtained with 1.00 eq. of NaOH have an aspect ratio of 44  $(44.0 \,\mu\text{m} \times 1.0 \,\mu\text{m})$  or  $21.1 \,(38.0 \,\mu\text{m} \times 1.8 \,\mu\text{m})$ , while the disks obtained with  $2.00 \,\text{eq}$ . NaOH result in 7.5 µm by 1.3 µm particles (AR: 5.7). The semicircular disks obtained with 1.25 eq. and 1.50 eq. NaOH yielded particles with aspect ratios of 35.8  $(14.3 \,\mu\mathrm{m} \times 0.4 \,\mu\mathrm{m})$  and 21.0  $(25.2 \,\mu\text{m} \times 1.2 \,\mu\text{m})$  as shown in Figure 2 (e) and Figure S2 (c).

The main goal for the synthesis optimization was the growth of high aspect ratio hexagonal  $\beta$ -NaYF disks with heights below 1 µm as levitated sensors in dual beam optical traps. The particles obtained with MIDA and the addition of 1.00 eq. of NaOH resulting in a pH just below the inflection point are 44 µm wide and 1 µm high, resulting in an aspect ratio of 44, which is an increase in width of over eight and in aspect ratio of over four times greater compared to previously reported syntheses using EDTA, citrate or other organic additives. The crystallographic orientation of the particles, indicated in Figure 2 (f), was investigated using electron backscatter diffraction (EBSD), the results are summarized in **Figure S4**. The minimum growth velocity over 72 h is calculated to be 260 nm h<sup>-1</sup> to 310 nm h<sup>-1</sup> along the  $\{11\bar{2}0\}$  directions and 225 nm h<sup>-1</sup> to 270 nm h<sup>-1</sup> for the  $\{1\bar{1}00\}$  family of directions. The growth velocity towards the basal plane  $\{0001\}$  family of directions on the other hand is only 5 nm h<sup>-1</sup> to 15 nm h<sup>-1</sup>. Interestingly, the best results for both MIDA and EDTA are obtained when half of the carboxylic acid groups are deprotonated, i.e. 1.00 eq. NaOH per MIDA molecule or 2.00 eq. NaOH per EDTA molecule.

As mentioned in the introduction, MIDA offers a bigger optimization parameter space than EDTA due to being more soluble in water. This allows for the growth of  $\beta$ -NaYF microparticles with different morphologies, from rods over disks to semicircular geometries. Unfortunately, the adjustability regions appear to be rather small, complicating the optimization for any desired particle morphologies or dimensions. This is especially true for the 1 eq. synthesis, as illustrated by the different results obtained just above and below the pH inflection point of MIDA. Furthermore, the use of MIDA resulted in phase mixtures for most of the experiments carried out here, which is not commonly observed when using EDTA. Lastly, the MIDA system is much more dependent on initial conditions than the EDTA counterpart. Using old Teflon liners (used once for another MIDA trial) led to observable changes in size, morphology and

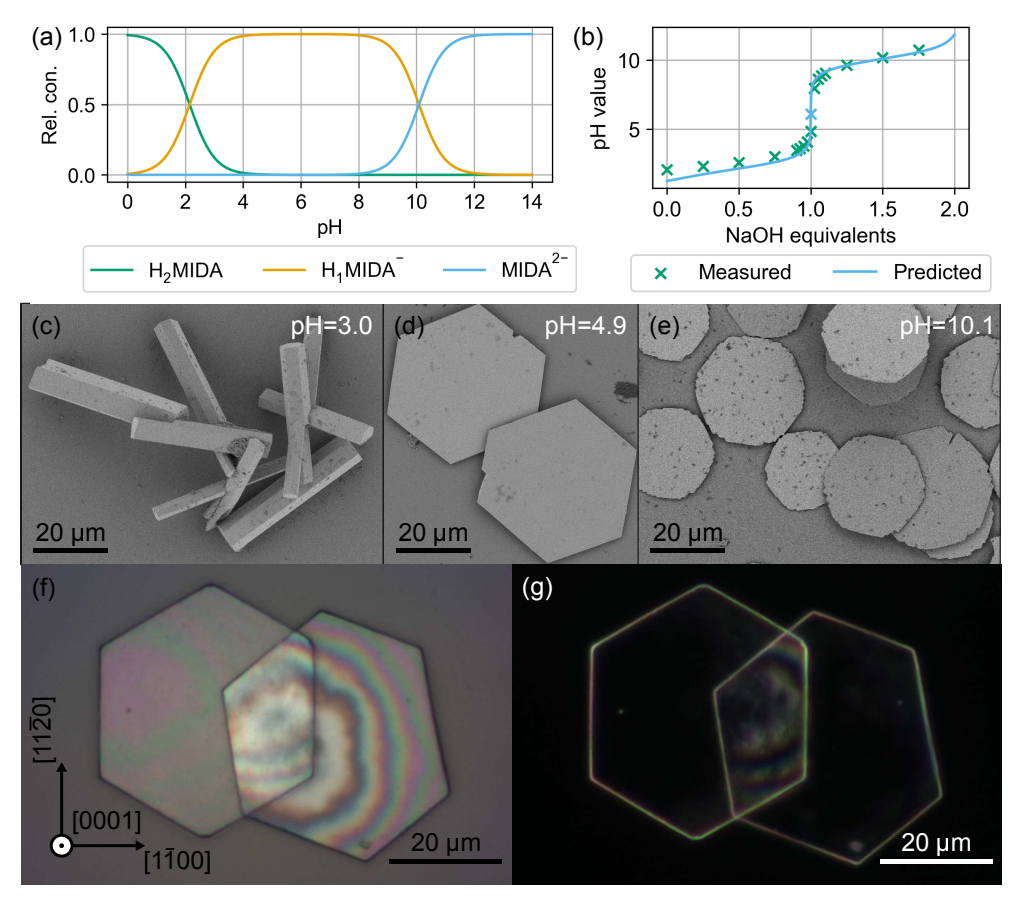


Figure 2: Calculated relative abundances of the different ionic MIDA species depending on pH (a). Predicted and measured pH value for a MIDA solution after the addition of NaOH. The inflection point, marked as blue cross, is calculated to be at a pH value of 6.1. The p $K_a$  values of MIDA are 2.146 and 10.088 (b) [34]. Hydrothermal synthesis results using MIDA in different protonation states by the addition of 0.75 eq. (c), 1.00 eq. (d) and 1.50 eq. (e) of sodium hydroxide. Optical bright- (f) and darkfield (g) images of the  $\beta$ -NaYF disks obtained with Na<sub>1.00</sub>MIDA. Crystallographic directions for the left particle are given in the optical brightfield image.

aspect ratio. A 1.00 eq. MIDA synthesis with pH of 4.1 resulted in inhomogeneous hexagonal disks with aspect ratios of 24 and sizes of  $(30.9\,\mu\text{m}\times1.3\,\mu\text{m})$  compared to  $(44.0\,\mu\text{m}\times1.0\,\mu\text{m})$ , AR: 44). In typical EDTA syntheses, the morphologies and aspect ratios are maintained and only the overall particle size is affected. These behaviors could be caused by altered heterogeneous nucleation rates as a result of an increase in the surface area and roughness of the Teflon liners.

Hexagonal β-NaYF disks grown using EDTA have the tendency to show curvature across the basal plane of the hexagonal disk, also known as lensing. It has been hypothesized that the curvature is due to terrace growth [31]. Basal plane curvature is significantly reduced in hexagonal disks synthesized using MIDA as shown in **Figure 3**. While the MIDA disks are

Table 1: Experimental conditions and results of the MIDA assisted hydrothermal  $\beta$ -NaYF synthesis.

-	NaOH [eq.]	рН	Phase	Morphology	Size [µm]	Aspect Ratio
	0.00	2.1	$YF_3, \beta$	Rods	$3.1 \pm 1.4 \times 15.6 \pm 5.7$	0.2
	0.50	2.6	$YF_3, \beta$	Rods	$3.1 \pm 0.6 \times 16.8 \pm 4.2$	0.2
	0.75	3.0	α, β	Rods	$8.7 \pm 1.9 \times 42.1 \pm 3.5$	0.2
	1.00	4.9	α, β	Hexagonal disks	$44.0 \pm 1.1 \times 1.0 \pm 0.1$	44.0
	1.00	7.7	β	Hexagonal disks	$38.0 \pm 5.2 \times 1.8 \pm 0.3$	21.1
	1.25	9.6	α, β	Circular disks	$14.3 \pm 6.8 \times 0.4 \pm 0.2$	35.8
	1.50	10.1	α, β	Circular disks	$25.2 \pm 2.4 \times 1.2 \pm 0.1$	21.0
	2.00	11.7	β	Hexagonal disks	$7.4 \pm 0.7 \times 1.3 \pm 0.2$	5.7

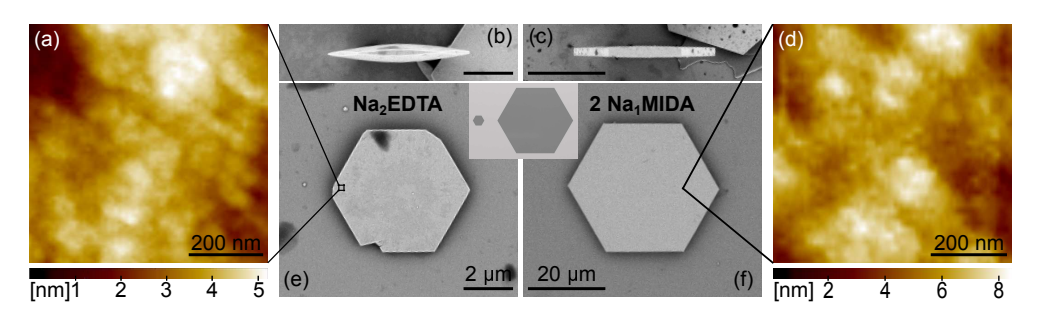


Figure 3: Size, morphology and surface comparison of Na<sub>2.00</sub>EDTA  $\beta$ -NaYF ((a), (b), (e)) and Na<sub>1.00</sub>MIDA  $\beta$ -NaYF ((c), (d), (f)). AFM surface characterization ((a), (d)), SEM side ((b), (c)) and top ((e), (f)) view, the inset illustrates the particle dimensions to scale.

virtually flat (radius of curvature approaching infinity) the synthesized EDTA microparticles show increased heights toward the center of the disks corresponding to a radius of curvature of roughly 14 µm. Both morphologies have potential applications as laser refrigerated microoptics, the EDTA particles are biconvex lenses with a calculated focal distance of roughly 14.4 µm. In contrast the flat surface of the MIDA disks could enable planar waveguiding of four different optical modes at a wavelength of 1020 nm. Atomic force microscopy (AFM) was used to compare the surfaces resulting from the different organic additives. For three different positions on two Na<sub>2.00</sub>EDTA  $\beta$ -NaYF disks a roughness average ( $R_a$ ) of (4.2 ± 1.8) nm and root-mean-square roughness ( $R_q$ ) of (4.3 ± 1.8) nm were obtained. A similar analysis of Na<sub>1.00</sub>MIDA disks yielded an  $R_a$  of (4.7 ± 1.2) nm and an  $R_q$  of (4.9 ± 1.1) nm showing a comparable surface roughness when using MIDA instead of EDTA, as shown in Figure 3 (a) and (d).

The size of the  $\beta$ -NaYF hexagonal disks synthesized here is large enough to enable single-crystal X-ray diffraction measurements. The particle investigated was observed to be a triplet with rotational twinning around the z-axis of 114.4° and 171.3°. The measured diffraction pattern best matched the P\bar{6}2c (\#190) space group after refinement (see **Figure S1** (a) and (b)). The sodium ions appear to be disordered on the c-axis with two locations at [000] and [000.5]. To the best of our knowledge, this structure has not been reported for \beta-NaYF and is of higher symmetry than the commonly discussed P\bar{6} (\#174), P\bar{6}2m (\#189) and P6\_3m (\#176) space groups [35, 36, 37, 38, 39, 40]. Following the notation from Kr\bar{a}mer et al. (2004)[39] we found a composition of Na<sub>0.75</sub>M<sub>1.75</sub>F<sub>6</sub> (Na<sub>3x</sub>M<sub>2-x</sub>F<sub>6</sub> with x = 0.25) and M constituted of

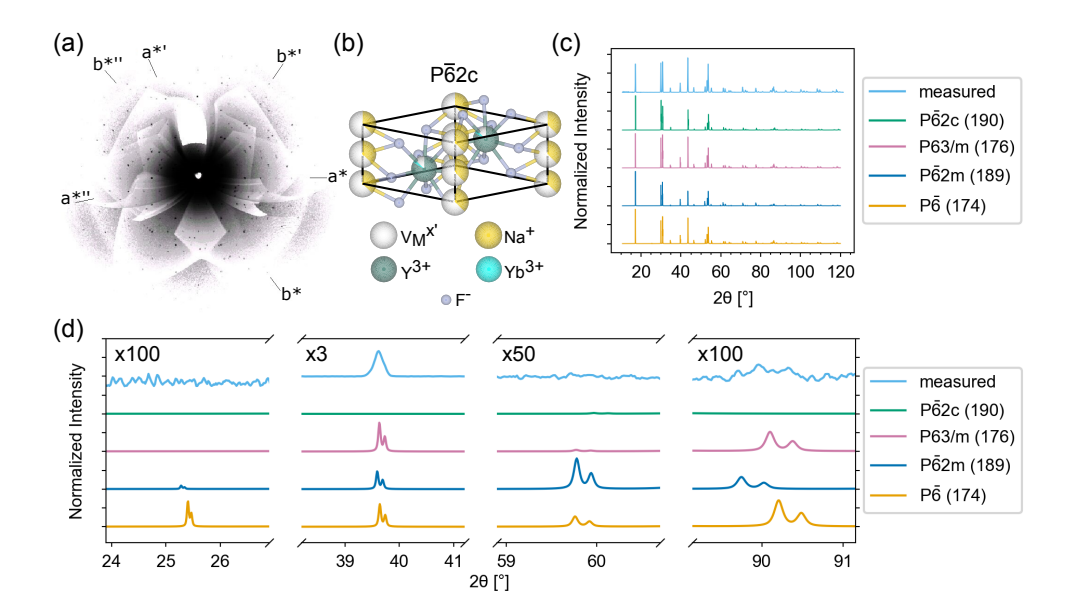


Figure 4: (hk0) Burger projection calculated from the single crystal X-ray diffraction images of the measured Na<sub>1.00</sub>MIDA  $\beta$ -NaYF drilling (a) and packing of the resulting refined crystal structure with P62c space group at 100 K (b). Comparison of experimental and predicted powder X-ray diffraction patterns for published crystal structures in full view (c) and zoomed in for crucial diffractions (d).

94.3 % Y<sup>3+</sup> and 5.7 % Yb<sup>3+</sup>. Complementary X-ray fluorescence (XRF) measurements showed a doping concentration of  $(8.5 \pm 0.4)$  % and detected no other lanthanides in the sample. A representative XRF spectrum is presented in Figure S5. Predicted powder XRD patterns and experimentally obtained data are presented in panels (c) and (d) of Figure S1. It becomes apparent that the observed diffraction peak around  $40^{\circ} 2\Theta$  is not predicted for the P62c space group, this is due to the fact that the corresponding (111) diffraction has a structure factor of zero caused by symmetry. The sodium ion disorder is only taken into account by average lattice occupancies and could potentially be the reason for a non-zero (111) diffraction intensity. The (111) diffraction is captured by the other published space groups ( $P\bar{6}$ ,  $P\bar{6}2m$  and  $P6_3m$ ), but unlike the proposed P62c space group, these also predict diffraction peaks that are not experimentally observed as shown in Figure S1 (d). The measured powder XRD data clearly show texturing and preferred orientation effects that distort relative intensities and, unlike the single crystal data, represent an ensemble average containing phase impurities, which could explain the observed diffraction around  $40^{\circ} 2\Theta$ . These phase impurities could be caused by the non-stoichiometry and local disturbances of the β-NaYF crystal structure. Because of the large surface area of the crystals, surface effects, like reconstructions, could alter the symmetry as well. Hypothetically β-NaYF could exist in different crystal structures depending on the nonstoichiometry index x, which might be altered during growth, for example due to depletion of the precursor solution. Different synthetic conditions could further enhance the effects and different methods (hydrothermal, thermal coprecipitation, or thermal decomposition) even more so. This could be one of the reasons why several different crystal structures have been reported for  $\beta$ -NaYF.

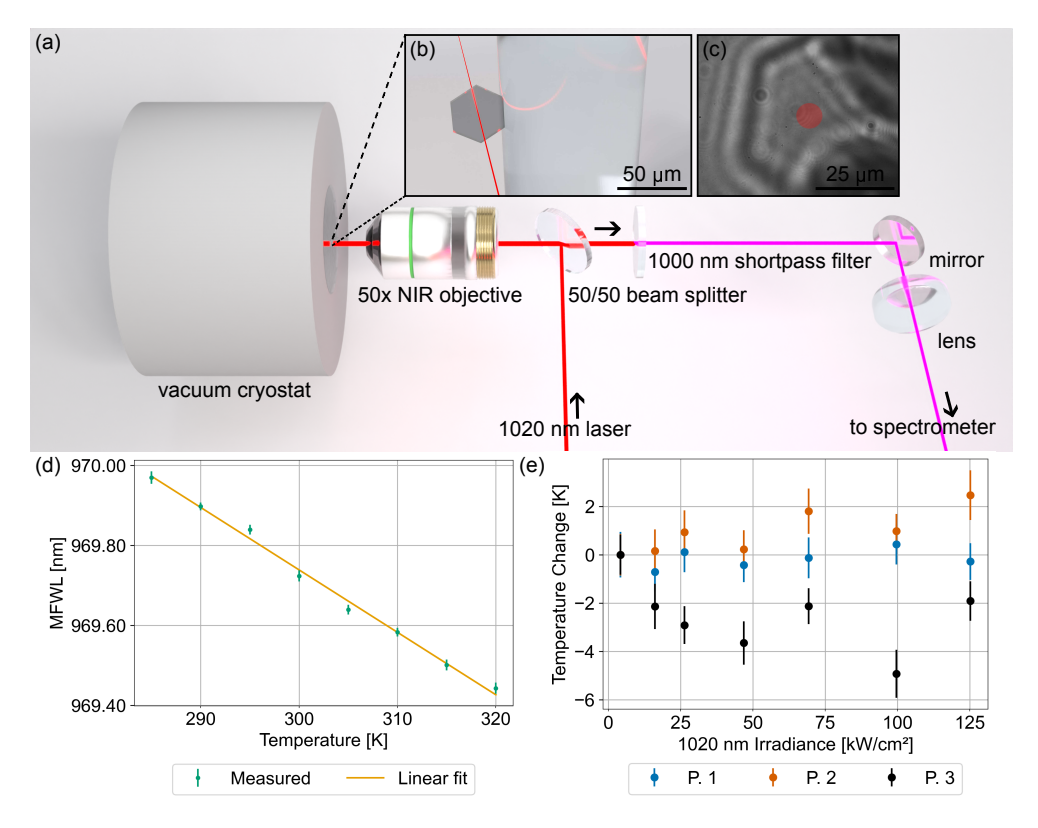


Figure 5: Schematic of the experimental setup used for the mean fluorescence wavelength temperature calibration and laser power dependent laser refrigeration trials (a). Illustration (b) and optical image (c) of a  $\beta$ -NaYF disk mounted on a fiber core to minimize substrate interactions. The illumination spot, with a size of 5 µm, is virtually overlaid as a red circle. Measured temperature calibration curve (d) and 1020 nm power-dependent temperature change of three different particles (b).

Beyond controlling the size and morphology, the synthesis was designed to maintain the laser refrigeration capabilities of  $\beta$ -NaYF through substitutional doping with Yb<sup>3+</sup>. In order to assess the temperature change of the Na<sub>1.00</sub>MIDA  $\beta$ -NaYF disks, power dependent anti-Stokes photoluminescence spectroscopy was performed on six different single crystals after calcination in air. A typical spectral response and the integration range for the mean fluorescence wavelength (MFWL) analysis are shown in **Figure S6**. Temperature calibration of the MFWL was achieved by measuring a particle at the lowest irradiance at different temperatures in a cryostat, the linear fit coefficients are (974.4  $\pm$  0.2) nm and (-15.6  $\pm$  0.5) pm K<sup>-1</sup> (see **Figure 5**). It should be noted that due to experimental limitations (detection filter cutoff at 1000 nm the MFWL is underestimated. Nonetheless, the measured value accurately tracks the temperature. Representative results of the power-dependent measurements are shown in Figure 5 (e). While two particles showed slight heating under increasing 1020 nm irradiance ((1.5  $\pm$  0.8) K and (2.5  $\pm$  1.0) K), three particles showed no significant temperature change ((-0.1  $\pm$  0.9) K, (0.2  $\pm$  0.7) K and (-0.3  $\pm$  0.8) K) and one particle cooled by (-4.9  $\pm$  1.0) K. These results

were obtained without any optimization of the dopant concentration or postsynthesis treatments like shelling, which have been shown to be able to greatly enhance quantum yields in upconversion nanoparticles and cooling efficiencies of  $\beta$ -NaYF nanoparticles [41, 16, 42, 43, 44]. The low cooling efficiency and percentage of refrigerating particles observed here are also seen for β-NaYF hydrothermally synthesized using EDTA and can potentially be attributed to the incorporation of OH<sup>-</sup> ions into the host lattice. Thermal decomposition and thermal coprecipitation, the other common synthesis methods, lead to better laser refrigeration and optical properties [44], but cannot readily produce microparticles with sizes and shapes designed for specific applications. The particle-to-particle differences observed during the laser refrigeration trials are confirmed by the inhomogeneous broadening observed at 4K for an ensemble of particles presented in Figure S7. Further, the presence of at least five peaks, with different mono- or biexponential PL decay rates (Figure S8), indicates different local environments of the Yb<sup>3+</sup> dopant. This could be caused by different non-stoichiometries, crystal structures or Yb-ion interactions with adjacent dopants or surface defects. The measured integrated intensity drop from 4 K to 298 K indicates the presence of increasing nonradiative decay rates and underline the problems of optical quality for the hydrothermal synthesis presented here. However, some individual β-NaYF particles show sufficient quality to achieve laser refrigeration. Further studies investigating the defect and crystal structure as well as non-stoichiometry might allow for an improvement in the laser refrigeration efficiency of hydrothermally grown β-NaYF microparticles.

#### 3 Conclusion

The substitution of ethylenediaminetetraacetic acid (EDTA) with methyliminodiactetic acid (MIDA) in hydrothermal synthesis allows for the growth of hexagonal β-NaYF disks with higher aspect ratios (44) and larger sizes (44.0  $\mu$ m  $\times$  1.0  $\mu$ m) than those previously reported (5  $\mu$ m  $\times$  $\sim$ 500 nm) resulting in an aspect ratio of 10.5 [31]. While different protonation states of MIDA allow for the synthesis of rods and novel semicircular disks, the adjustment ranges are small and byproducts like α-NaYF and YF<sub>3</sub> are present. The surface roughness of the disks obtained with MIDA is comparable to those synthesized with EDTA, but the MIDA microparticles have flat basal planes, unlike the lensing observed with EDTA. Single crystal XRD results indicate a P62c (#190) space group of the 44.0 μm β-NaYF particles, which has not been reported in the literature. Deviations of experimentally obtained powder diffraction data are attributed to non-stoichiometry and local distortions. The crystal structure and non-stoichiometry of β-NaYF is hypothesized to depend on specific synthesis conditions and processing parameters. Laser refrigeration was observed with temperature decreases of  $(-4.9 \pm 1.0)$  K based on the anti-Stokes photoluminescence of Yb<sup>3+</sup>-dopants in one of six particles. The large aspect ratio of these microcrystals makes them promising candidates for future applications in optically levitated gravitational wave sensing and microoptics.

### 4 Experimental Section

Synthesis of  $\beta$ -NaYF YCl<sub>3</sub>·6 H<sub>2</sub>O (99.9%), YbCl<sub>3</sub>·6 H<sub>2</sub>O (99.998%), methyliminodiactetic acid (MIDA, 99%) and ethylenediaminetetraacetic acid (EDTA, 99.995%) were purchased from Sigma-Aldrich. NaOH (99.5%) was purchased from Fisher Scientific and NaF (99.5%) was obtained from EMD Chemicals. Ultrapure water was used for all experiments

(Barnstead GenPure). In a typical synthesis  $4\,\mathrm{mL}$  of a  $0.25\,\mathrm{M}$  aqueous rare-earth solution (90 % Y and 10 % Yb) were chelated with  $5\,\mathrm{mL}$  MIDA solution in an autoclave liner for  $10\,\mathrm{min}$  while stirring. The protonation state of MIDA was controlled by dissolving 2 mmol in a total volume of  $5\,\mathrm{mL}$  of a mixture of  $\mathrm{H_2O}$  and  $5\,\mathrm{M}$  NaOH.  $5\,\mathrm{mL}$  of  $0.8\,\mathrm{M}$  NaF solution was added, and the solution left to nucleate for 30 min under stirring. After the stir bar was removed, the liner was placed in an autoclave (Parr Instruments 4747) and a preheated oven at  $220\,^{\circ}\mathrm{C}$  for  $72\,\mathrm{h}$ . After the autoclave naturally cooled to room temperature, the precipitate was collected and washed three times with 30 mL of  $\mathrm{H_2O}$  and EtOH respectively. The resulting product was dried at roughly  $80\,^{\circ}\mathrm{C}$  overnight. Synthesis using EDTA followed the same procedure, 2 mmol MIDA were replaced by 1 mmol EDTA. If a mixture of  $\alpha\mathrm{-NaYF}$  and  $\beta\mathrm{-NaYF}$  was present, the  $\alpha\mathrm{-NaYF}$  particles were removed by dispersion in EtOH followed by supernatant removal for three times. Finally, the powder was calcined at  $300\,^{\circ}\mathrm{C}$  for  $4\,\mathrm{h}$  in air to remove surface ligands and adsorbents.

Host Characterization Scanning electron microscope (SEM) images were obtained on a Thermo Fisher Scientific Apreo 2 S using an accelerating voltage of  $2\,\mathrm{kV}$  and current of  $13\,\mathrm{pA}$ . Powder X-ray diffraction (XRD) data were obtained on a Bruker D8 Discover instrument. X-ray fluorescence was measured on a Bruker M4 Tornado equipped with a rhodium source operated at  $50\,\mathrm{keV}$  and  $600\,\mathrm{pA}$ . Quantitative data analysis of lanthanide ion concentrations was obtained with the corresponding Bruker software. Atomic force microscopy (AFM) images were collected on a Dimension Icon AFM (Bruker) in tapping mode using Multi75Al probes (Budget Sensors). All images were recorded in air at room temperature. Offline data processing and analysis were done using Gwyddion software. Single-crystal XRD measurements were conducted on a Bruker APEX II diffractometer using molybdenum (Mo) radiation and an optical Miracol X-ray collimator. The sample was mounted on a loop with oil. Data were collected at  $-173\,^{\circ}\mathrm{C}$ . The crystal-to-detector distance was 40 mm and exposure time was 60 seconds per frame for all sets using a scan width of  $1^{\circ}$ . More information on data processing and analysis can be found in the supporting information.

Optical Characterization The 1020 nm laser power-dependent temperature change of single particles was evaluated using mean fluorescence wavelength thermometry [33], based on temperature-dependent spectral changes very similar to two-band differential luminescence thermometry [45]. The samples were loaded onto an optical fiber core, mounted in a liquid nitrogen cooled vacuum cryostat and irradiated through a 50 x NIR-corrected microscope objective (50X Mitotuyo Plan Apo NIR Infinity Corrected) with a 1020 nm laser diode (QPhotonics, QDFBLD-1020-400). The optical response was measured by an EM-CCD (BLAZE 100-HR, Princeton Instruments) in an epifluorescence setup after passing a 1000 nm short-pass filter (see Figure 5).

Temperature-dependent photoluminescence measurements were conducted on powder samples of the material prepared as a mull suspension by mixing dry powder with polydimethylsiloxane then sandwiched between two sapphire disks. The sample was loaded into a closed-cycle helium cryostat and measured under high vacuum  $(1 \times 10^{-6} \,\mathrm{Pa})$ . Sample emission was focused into a monochromator with a spectral bandwidth of 0.1 nm for spectral data and 1 nm for time-resolved measurements. Spectra were collected using a liquid nitrogen-cooled silicon CCD camera and were corrected for instrument response. Time-resolved data was collected using a liquid nitrogen-cooled Hamamatsu InGaAs/InP NIR photomultiplier tube. Photoexcitation was performed using a tunable Ti:Sapphire laser at 942 nm, 150 mW cm<sup>-2</sup>, continuous-wave. For time-resolved experiments, the laser was at 942 nm, 500 nJ cm<sup>-2</sup>, 2 kHz, 1 µs pulse duration.

#### References

- [1] Bing Chen and Feng Wang. "Recent Advances in the Synthesis and Application of Yb-based Fluoride Upconversion Nanoparticles". In: *Inorganic Chemistry Frontiers* 7.5 (2020), pp. 1067–1081. DOI: 10.1039/c9qi01358j.
- [2] Karan Malhotra et al. "Lanthanide-Doped Upconversion Nanoparticles: Exploring A Treasure Trove of NIR-Mediated Emerging Applications". In: ACS Applied Materials & Interfaces (Jan. 2023). DOI: 10.1021/acsami.2c12370.
- [3] Baobao Zhang et al. "Luminescence Thermometry with Rare Earth Doped Nanoparticles: Status and Challenges". In: *Journal of Luminescence* 250 (Oct. 2022), p. 119110. DOI: 10.1016/j.jlumin.2022.119110.
- [4] Xiaohui Zhu et al. "Recent Progress of Rare-Earth Doped Upconversion Nanoparticles: Synthesis, Optimization, and Applications". In: *Advanced Science* 6.22 (Sept. 2019), p. 1901358. DOI: 10.1002/advs.201901358.
- [5] Bingzhu Zheng et al. "Rare-Earth Doping in Nanostructured Inorganic Materials". In: Chemical Reviews 122.6 (Jan. 2022), pp. 5519–5603. ISSN: 1520-6890. DOI: 10.1021/acs.chemrev.1c00644.
- [6] Ayush Khare. "A Critical Review on the Efficiency Improvement of Upconversion Assisted Solar Cells". In: *Journal of Alloys and Compounds* 821 (Apr. 2020), p. 153214. DOI: 10.1016/j.jallcom.2019.153214.
- [7] Ting Wang et al. "White-Light Whispering-Gallery-Mode Lasing from Lanthanide-Doped Upconversion NaYF4 Hexagonal Microrods". In: ACS Photonics 4.6 (May 2017), pp. 1539–1543. ISSN: 2330-4022. DOI: 10.1021/acsphotonics.7b00301.
- [8] Angel Fernandez-Bravo et al. "Continuous-Wave Upconverting Nanoparticle Microlasers". In: *Nature Nanotechnology* 13.7 (June 2018), pp. 572–577. ISSN: 1748-3395. DOI: 10.1038/s41565-018-0161-8.
- [9] Yawei Liu et al. "Controlled Assembly of Upconverting Nanoparticles for Low-Threshold Microlasers and Their Imaging in Scattering Media". In: ACS Nano 14.2 (Feb. 2020), pp. 1508–1519. ISSN: 1936-086X. DOI: 10.1021/acsnano.9b06102.
- [10] Markus P. Hehlen et al. "First Demonstration of an All-Solid-State Optical Cryocooler". In: Light: Science & Applications 7.1 (June 2018), p. 15. ISSN: 2047-7538. DOI: 10.1038/s41377-018-0028-7. (Visited on 11/10/2025).
- [11] Junwei Meng et al. "Realization of an All-Solid-State Cryocooler Using Optical Refrigeration". In: Tri-Technology Device Refrigeration (TTDR) III. Ed. by Richard I. Epstein et al. Orlando, United States: SPIE, May 2018, p. 10. DOI: 10.1117/12.2305195. (Visited on 11/10/2025).
- [12] Nancy Aggarwal et al. "Searching for New Physics with a Levitated-Sensor-Based Gravitational-Wave Detector". In: *Physical Review Letters* 128.11 (Mar. 2022), p. 111101. ISSN: 1079-7114. DOI: 10.1103/physrevlett.128.111101.

- [13] George Winstone et al. "Optical Trapping of High-Aspect-Ratio NaYF Hexagonal Prisms for kHz-MHz Gravitational Wave Detectors". In: *Physical Review Letters* 129.5 (July 2022), p. 053604. DOI: 10.1103/physrevlett.129.053604.
- [14] R. E. Thoma et al. "Phase Equilibria in the System Sodium Fluoride-Yttrium Fluoride". In: *Inorganic Chemistry* 2.5 (Oct. 1963), pp. 1005–1012. DOI: 10.1021/ic50009a030.
- [15] N. Menyuk, K. Dwight, and J.W. Pierce. "NaYF4: Yb,Er—an Efficient Upconversion Phosphor". In: Applied Physics Letters 21.4 (Aug. 1972), pp. 159–161. ISSN: 0003-6951, 1077-3118. DOI: 10.1063/1.1654325. (Visited on 05/09/2025).
- [16] Markus Haase and Helmut Schäfer. "Upconverting Nanoparticles". In: *Angewandte Chemie International Edition* 50.26 (June 2011), pp. 5808–5829. ISSN: 1433-7851, 1521-3773. DOI: 10.1002/anie.201005159. (Visited on 05/09/2025).
- [17] David Knowles, A. Cassanho, and H. P. Jenssen. "Optical Properties of Nd:NaYF4 and Ho:NaYF4". In: Advanced Solid State Lasers. Vol. 70. ASSL. OSA, 1989, p. CC7. DOI: 10.1364/assl.1989.cc7.
- [18] Annina Aebischer et al. "Structural and Spectroscopic Characterization of Active Sites in a Family of Light-Emitting Sodium Lanthanide Tetrafluorides". In: *Angewandte Chemie International Edition* 45.17 (Apr. 2006), pp. 2802–2806. ISSN: 1521-3773. DOI: 10.1002/anie.200503966.
- [19] Nikita A. Bogachev et al. "Lanthanide-Ion-Doping Effect on the Morphology and the Structure of NaYF4:Ln3+ Nanoparticles". In: *Nanomaterials* 12.17 (Aug. 2022), p. 2972. ISSN: 2079-4991. DOI: 10.3390/nano12172972. (Visited on 05/19/2025).
- [20] Huan Chen et al. "Enhanced High-Order Upconversion Luminescence of Hexagonal Phase NaYF 4:Yb 3+, Tm 3+ Crystals Coated with Homogeneous Shell". In: *Journal of Fluo-rine Chemistry* 174 (June 2015), pp. 70–74. ISSN: 00221139. DOI: 10.1016/j.jfluchem. 2015.02.019. (Visited on 05/19/2025).
- [21] Yongsheng Chen et al. "β-NaYF4:Er3+(10%) Microprisms for the Enhancement of a-Si:H Solar Cell near-Infrared Responses". In: Journal of Luminescence 132.9 (Sept. 2012), pp. 2247–2250. ISSN: 00222313. DOI: 10.1016/j.jlumin.2012.04.011. (Visited on 05/15/2025).
- [22] Junxiang Fu et al. "Enhanced Upconversion Luminescence of NaYF 4:Yb, Er Microprisms via La 3+ Doping". In: Optics & Laser Technology 88 (Feb. 2017), pp. 280-286.
  ISSN: 00303992. DOI: 10.1016/j.optlastec.2016.09.029. (Visited on 05/19/2025).
- [23] Shuwei Hao et al. "Controlled Growth along Circumferential Edge and Upconverting Luminescence of  $\beta$ -NaYF4: 20%Yb3+, 1%Er3+ Microcrystals". In: *Materials Chemistry and Physics* 137.1 (Nov. 2012), pp. 97–102. ISSN: 02540584. DOI: 10.1016/j.matchemphys. 2012.08.045. (Visited on 05/15/2025).
- [24] Chunxia Li et al. "Different Microstructures of β-NaYF<sub>4</sub> Fabricated by Hydrothermal Process: Effects of pH Values and Fluoride Sources". In: Chemistry of Materials 19.20 (Oct. 2007), pp. 4933–4942. ISSN: 0897-4756, 1520-5002. DOI: 10.1021/cm071668g. (Visited on 05/14/2025).
- [25] Elisa Ortiz-Rivero et al. "Laser Refrigeration by an Ytterbium-Doped NaYF 4 Microspinner". In: Small 17.46 (Sept. 2021), p. 2103122. DOI: 10.1002/smll.202103122.

- [26] Kedar Sahoo, Sudhir Ranjan, and Manoj Kumar. "Lattice-Strain Induced Photophysical Properties of NaYF4: Yb3+, Tm3+ Upconverting Phosphors". In: *Journal of Lumines-cence* 251 (Nov. 2022), p. 119249. ISSN: 00222313. DOI: 10.1016/j.jlumin.2022.119249. (Visited on 05/19/2025).
- [27] Sudipta Som et al. "Synthesis and Design of NaYF<sub>4</sub> Microprisms via a Microwave-assisted Approach for Highly Sensitive Optical Thermometry Applications". In: *Journal of the American Ceramic Society* 104.10 (Oct. 2021), pp. 5168–5181. ISSN: 0002-7820, 1551-2916. DOI: 10.1111/jace.17783. (Visited on 05/19/2025).
- [28] Junmei Wang et al. "Controlled Synthesis and Luminance Properties of Lanthanide-Doped  $\beta$ -NaYF4 Microcrystals". In: *Journal of Rare Earths* 33.4 (Apr. 2015), pp. 339–345. ISSN: 10020721. DOI: 10.1016/S1002-0721(14)60423-3. (Visited on 05/19/2025).
- [29] Yan Wang et al. "Synthesis of NaYF4 Microcrystals with Different Morphologies and Enhanced Up-Conversion Luminescence Properties". In: *Physical Chemistry Chemical Physics* 15.39 (2013), p. 16795. ISSN: 1463-9076, 1463-9084. DOI: 10.1039/c3cp52813h. (Visited on 05/15/2025).
- [30] Jianping Yang et al. "One-Step Hydrothermal Synthesis of Carboxyl-Functionalized Upconversion Phosphors for Bioapplications". In: Chemistry – A European Journal 18.43 (Oct. 2012), pp. 13642–13650. ISSN: 0947-6539, 1521-3765. DOI: 10.1002/chem.201202336. (Visited on 05/15/2025).
- [31] R. Greg Felsted et al. "Chemically Tunable Aspect Ratio Control and Laser Refrigeration of Hexagonal Sodium Yttrium Fluoride Upconverting Materials". In: Crystal Growth & Design 22.6 (May 2022), pp. 3605–3612. DOI: 10.1021/acs.cgd.1c01174.
- [32] Robert M. Smith and Arthur E. Martell. "Critical Stability Constants, Enthalpies and Entropies for the Formation of Metal Complexes of Aminopolycarboxylic Acids and Carboxylic Acids". In: Science of The Total Environment 64.1-2 (June 1987), pp. 125–147. ISSN: 00489697. DOI: 10.1016/0048-9697(87)90127-6. (Visited on 11/10/2025).
- [33] Danika R. Luntz-Martin et al. "Laser Refrigeration of Optically Levitated Sodium Yttrium Fluoride Nanocrystals". In: *Optics Letters* 46.15 (July 2021), p. 3797. DOI: 10.1364/ol.426334.
- [34] Nelson E. Ockerbloom and Arthur E. Martell. "Thermodynamic Dissociation Constants of Methylaminediacetic Acid and Dimethylethylenediaminediacetic Acid". In: *Journal of the American Chemical Society* 78.2 (Jan. 1956), pp. 267–270. ISSN: 0002-7863, 1520-5126. DOI: 10.1021/ja01583a004. (Visited on 05/28/2025).
- [35] Zhijun Wang et al. "Selected Synthesis of Cubic and Hexagonal NaYF4 Crystals via a Complex-Assisted Hydrothermal Route". In: *Journal of Crystal Growth* 290.1 (Apr. 2006), pp. 296–300. ISSN: 0022-0248. DOI: 10.1016/j.jcrysgro.2006.01.012.
- [36] P. P. Fedorov et al. "Soft Chemical Synthesis of NaYF4 Nanopowders". In: Russian Journal of Inorganic Chemistry 53.11 (Nov. 2008), pp. 1681–1685. ISSN: 1531-8613. DOI: 10.1134/s0036023608110028.
- [37] Bi-Qiu Liu et al. "Remarkable Enhancement of the Near-Infrared Upconversion Emission in the β-NaYF4:Yb3+/Tm3+ System with Controllable Morphology". In: Materials Research Bulletin 51 (Mar. 2014), pp. 180-184. ISSN: 0025-5408. DOI: 10.1016/j.materresbull.2013.11.057.

- [38] Monalisa Bessoi, Siba Soren, and Purnendu Parhi. "Rapid Microwave Mediated Hydrothermal Synthesis of Complex Ternary Fluorides". In: *Ceramics International* 42.2 (Feb. 2016), pp. 3697–3700. ISSN: 0272-8842. DOI: 10.1016/j.ceramint.2015.10.149.
- [39] Karl W. Krämer et al. "Hexagonal Sodium Yttrium Fluoride Based Green and Blue Emitting Upconversion Phosphors". In: Chemistry of Materials 16.7 (Mar. 2004), pp. 1244–1251. ISSN: 1520-5002. DOI: 10.1021/cm031124o.
- [40] Shili Gai et al. "Facile Synthesis and Up-Conversion Properties of Monodisperse Rare Earth Fluoride Nanocrystals". In: *Dalton Transactions* 41.38 (2012), p. 11716. ISSN: 1477-9234. DOI: 10.1039/c2dt30954h.
- [41] Guang-Shun Yi and Gan-Moog Chow. "Water-Soluble NaYF<sub>4</sub>:Yb,Er(Tm)/NaYF<sub>4</sub>/Polymer Core/Shell/Shell Nanoparticles with Significant Enhancement of Upconversion Fluorescence". In: *Chemistry of Materials* 19.3 (Feb. 2007), pp. 341–343. ISSN: 0897-4756, 1520-5002. DOI: 10.1021/cm062447y. (Visited on 05/20/2025).
- [42] Stefan Fischer et al. "Precise Tuning of Surface Quenching for Luminescence Enhancement in Core-Shell Lanthanide-Doped Nanocrystals". In: Nano Letters 16.11 (Nov. 2016), pp. 7241-7247. ISSN: 1530-6984, 1530-6992. DOI: 10.1021/acs.nanolett.6b03683. (Visited on 05/20/2025).
- [43] Christian Würth et al. "Quantum Yields, Surface Quenching, and Passivation Efficiency for Ultrasmall Core/Shell Upconverting Nanoparticles". In: *Journal of the American Chemical Society* 140.14 (Apr. 2018), pp. 4922–4928. ISSN: 0002-7863, 1520-5126. DOI: 10.1021/jacs.8b01458. (Visited on 09/08/2025).
- [44] Cyril Laplane et al. "Inert Shell Coating for Enhanced Laser Refrigeration of Nanoparticles: Application in Levitated Optomechanics". In: ACS Photonics 11.3 (Mar. 2024), pp. 963–968. ISSN: 2330-4022. DOI: 10.1021/acsphotonics.3c01065.
- [45] W. M. Patterson et al. "Measurement of Solid-State Optical Refrigeration by Two-Band Differential Luminescence Thermometry". In: *Journal of the Optical Society of America B* 27.3 (Mar. 2010), p. 611. ISSN: 0740-3224, 1520-8540. DOI: 10.1364/JOSAB.27.000611. (Visited on 05/20/2025).

## Supplemental Materials: Hydrothermal Synthesis of Ultra-high Aspect Ratio $\beta$ -NaYF Disks via Methyliminodiacetic Acid (MIDA)

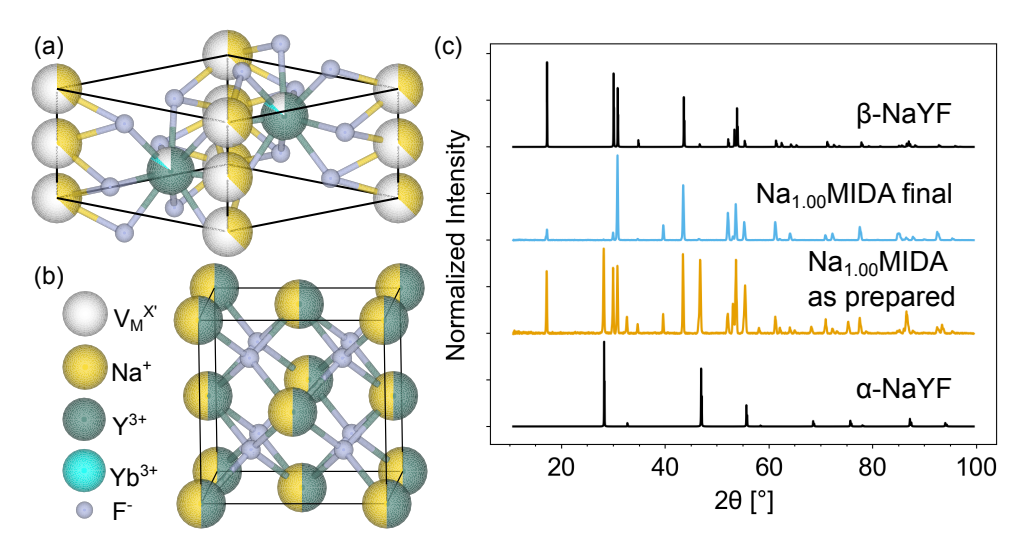


Figure S1: Crystal structure of  $\beta$ - (a) and  $\alpha$ -NaYF (b) [1]. XRD patterns (c) of Na<sub>1.00</sub>MIDA synthesis before and after  $\alpha$ -NaYF removal and calcination.

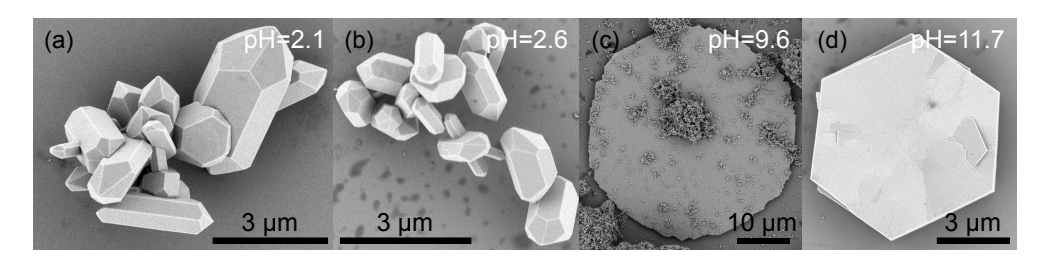


Figure S2: Hydrothermal synthesis results using MIDA in different protonation states by the addition of 0.00 eq. (a), 0.50 eq. (b), 1.25 eq. (c) and 2.00 eq. (d).

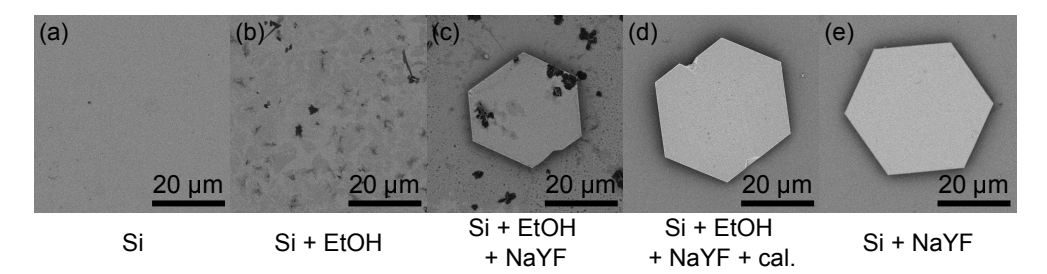


Figure S3: SEM images of cleaned Si substrate (a), Si substrate after drop casting ethanol (b), MIDA  $\beta$ -NaYF drop cast from ethanol (c), drop cast from ethanol and calcined (d) and dry attached to the Si substrate (e).

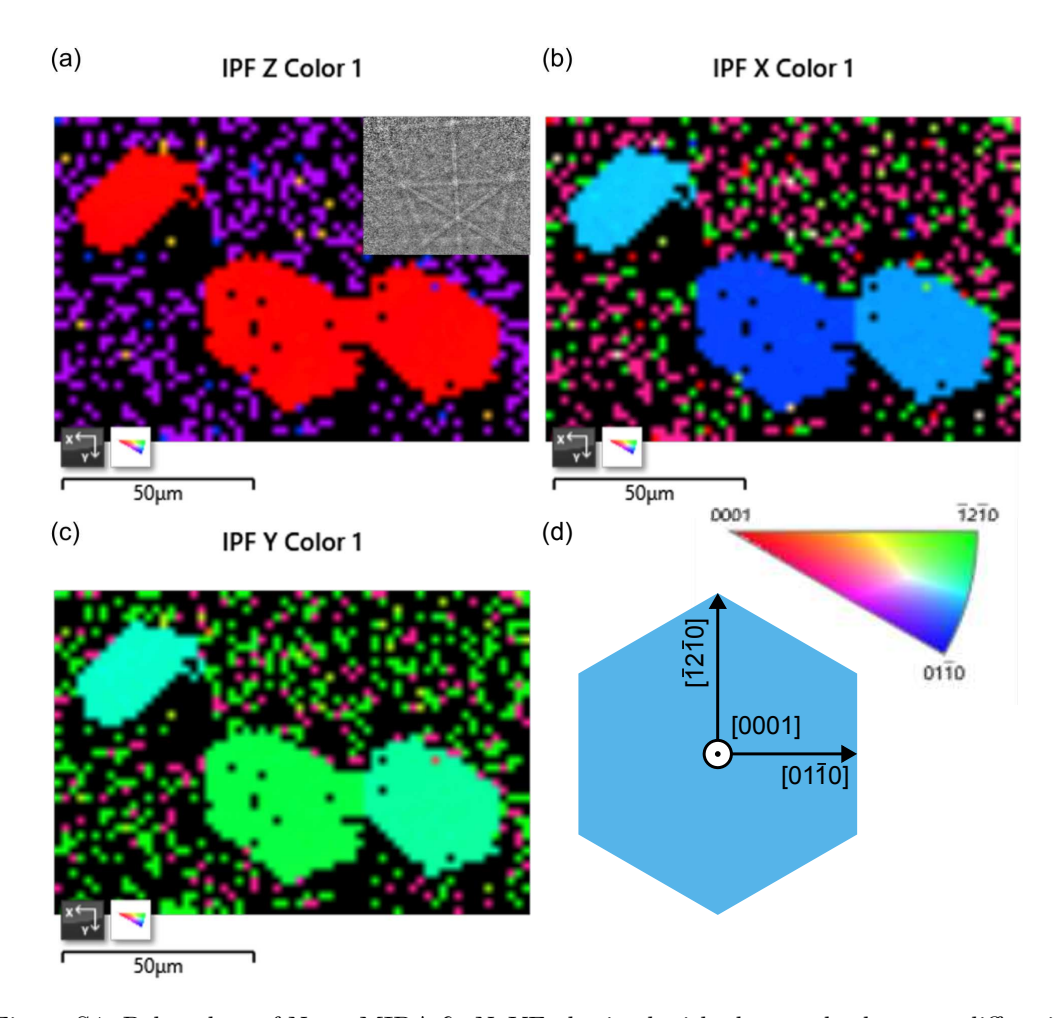


Figure S4: Polar plots of  $Na_{1.00}MIDA$   $\beta-NaYF$  obtained with electron backsactter diffraction (EBSD) (a)-(c) and crystallographic orientation of the hexagonal particles (d). The inset in (a) shows a representative single point Kikuchi pattern.

Single crystal XRD data processing and analysis Data collection was 96.1 % complete to 25° in  $\vartheta$ . A total of 250 merged reflections were collected covering the indices, -7 <= h <= 7, -8 <= k <= 9, -5 <= l <= 5. 137 reflections were symmetry independent and the  $R_{int} = 0.0166$  indicated that the data was of excellent quality (average 0.07). Indexing and unit cell refinement indicated a primitive hexagonal lattice. The space group was found to be P62c (#190).

The data appeared to be of a drilling (CELL\_NOW [2]) and after multi-domain integration (SAINT, SADABS within the APEX2 software package by Bruker [3]) the data was merged utilizing TWINABS [4].

Solutions by direct methods (SHELXT [5, 6] or SIR97 [7, 8]) produced a complete heavy atom phasing model consistent with the proposed structure. The structure was completed by difference Fourier synthesis with SHELXL [9, 10]. Scattering factors are from Waasmair and Kirfel [11]. All atoms were refined anisotropically by full-matrix least-squares.

The sodium appears disordered on the c-axis with two locations at  $[0\ 0\ 0]$  and  $[0\ 0\ 0.5]$  (symmetry related to the actual coordinates in the refinement). The sodium site appearntly did not contain any yttrium and vice versa. The occupancies were fitted from satisfying equation 6 = occup.(Na) + 3\*occup.(Y) to ensure the sum of the cations charges adds up to +6. The space group is non-centrosymmetric but the sample appears to be a racemate with Flack parameter of 0.5(7). No higher symmetry was found.

Table S1 summarizes the data collection details.

Table S1: Crystallographic data for the  $\mathrm{Na}_{1.00}\mathrm{MIDA}~\beta-\mathrm{NaYF}$  structure provided.

Empirical formula Formula weight Temperature Wavelength Crystal system Space group Unit cell dimensions	$F_6Na_{0.75}Y_{1.65}Yb_{0.10}$ $295.25 \text{ g mol}^{-1}$ 100(2)  K 0.71073  Å Hexagonal P - 6 2  c $a = 5.9451(5) \text{ Å}$ $\alpha = 90^{\circ}$ $b = 5.9451(5) \text{ Å}$ $\beta = 90^{\circ}$	
	$c = 3.5054(4) \text{ Å} \qquad \beta = 120^{\circ}$	
Volume	$107.30(2) \text{ Å}^3$	
Z	1	
Density (calculated)	$4.569 { m Mg m}^{-3}$	
Absorption coefficient	$24.512 \text{ mm}^{-1}$	
F(000)	134	
Crystal size	$0.040 \times 0.035 \times 0.002 \text{ mm}^3$	
Theta range for data collection	$3.958 \text{ to } 32.776^{\circ}$	
Index ranges	$-7_{i}=h_{i}=7, -8_{i}=k_{i}=9, -5_{i}=l_{i}=5$	
Reflections collected	250	
Independent reflections	137 [R(int) = 0.0166]	
Completness to thetha = $25.242^{\circ}$	96.1%	
Refinement method	Full-matrix least-squares on $F^2$	
Data / restraints / parameters	137 / 1 / 15	
Goodness-of-fit on $F^2$	1.396	
Final R indices [I¿2sigma(I)]	R1 = 0.0318, wR2 = 0.0863	
R indices (all data)	R1 = 0.0319, wR2 = 0.0863	
Absolute structure parameter	0.51(7)	
Largest diff. peak and hole	1.489 and -1.177 e. Å $^3$	

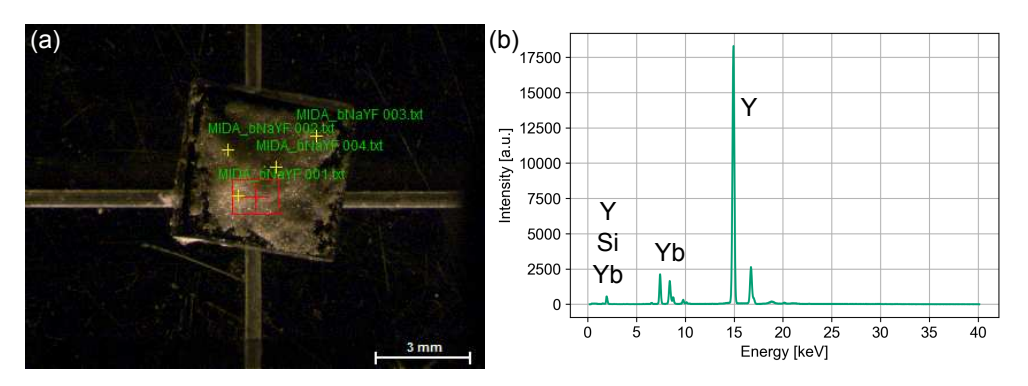


Figure S5: Microscope image of Na<sub>1.00</sub>MIDA  $\beta$ -NaYF drop cast from EtOH on SI (a) and representative X-ray fluorescence spectrum of the sample (b). The average Yb<sup>3+</sup> doping concentration from four point measurements was  $(8.5 \pm 0.4) \%$ .

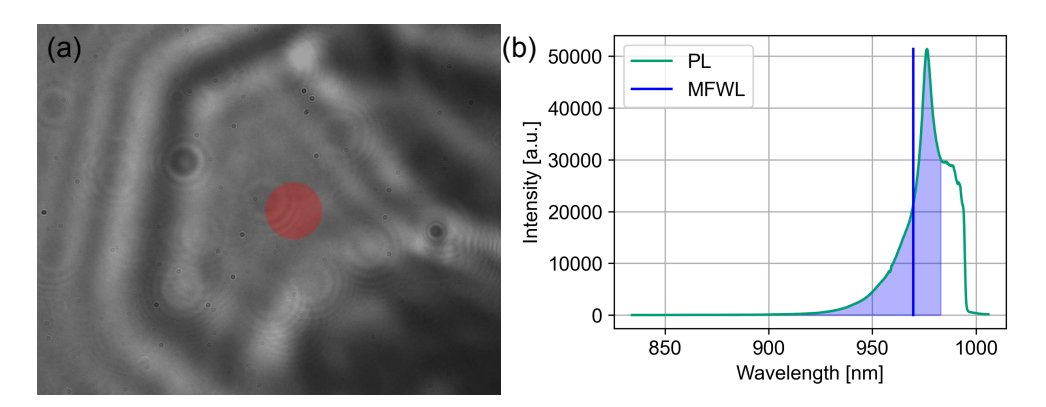


Figure S6: Image of a  $Na_{1.00}MIDA~\beta-NaYF$  particle on a fiber core with the 1020 nm focussed laser spot indicated in red (a). Spectral anti-Stokes response of the Yb<sup>3+</sup> dopant and mean fluorescence wavelength (MFWL) integration range (b).

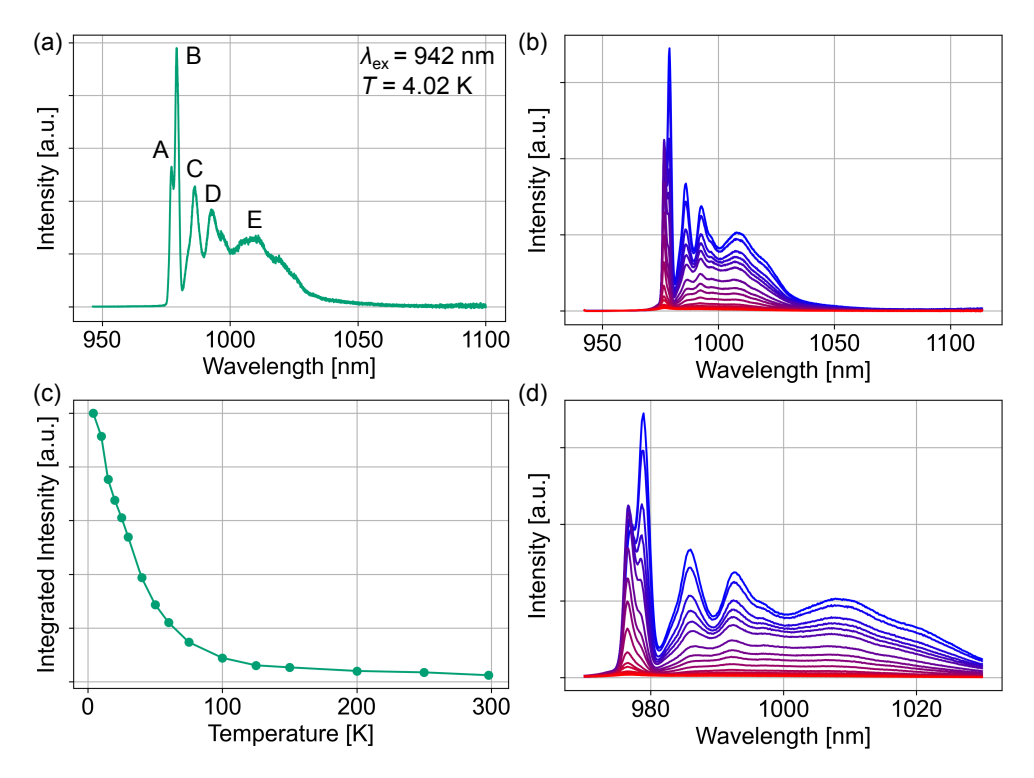


Figure S7: Low temperature PL spectrum of an ensemble of  $Na_{1.00}MIDA~\beta-NaYF$  particles under 942 nm continuous wave excitation (a). Variable temperature PL from 4 K to 298 K (blue to red) (b). Temperature-dependent integrated PL intensity over the entire spectral region (c). Zoomed in version of variable temperature PL (d).

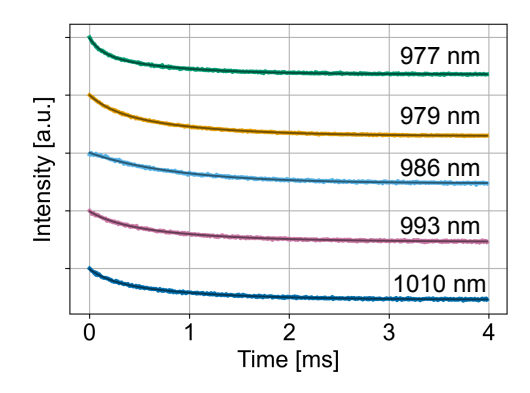


Figure S8: PL decay plots of the A, B, C, D and E peaks labeled in Figure S7, excited using a 942 nm source with 2000 Hz frequency and 1 µs pulse. Black curves are fit using a mono-(C) or biexponential decay functions (A, B, D, E).

Table S2: Fitting results using mono- or biexponetial decays for the time-resolved photoluminescence of peaks A-E. Relative integrated intensities are given in brackets.

λ [nm]	$\tau_1 [\mathrm{ms}]$	$\tau_2 \; [\mathrm{ms}]$
977	$0.765 \ (72 \%)$	0.128 (28 %)
979	0.940~(82%)	0.229~(18%)
986	0.895~(100%)	N/A
993	0.991~(83%)	0.263~(17%)
1010	0.948~(82%)	$0.197\ (18\%)$

#### References

- [1] Zhijun Wang et al. "Selected Synthesis of Cubic and Hexagonal NaYF4 Crystals via a Complex-Assisted Hydrothermal Route". In: *Journal of Crystal Growth* 290.1 (Apr. 2006), pp. 296–300. ISSN: 0022-0248. DOI: 10.1016/j.jcrysgro.2006.01.012.
- [2] George Michael Sheldrick. CELL\_NOW. 2005.
- [3] Bruker. APEX2 (Version 2.1-4), SAINT (Version 7.34A), SADABS (Version 2007/4). 2007.
- [4] George Michael Sheldrick. TWINABS. 2007.
- [5] George M. Sheldrick. "A Short History of SHELX". In: Acta Crystallographica Section A Foundations of Crystallography 64.1 (Dec. 2007), pp. 112–122. ISSN: 0108-7673. DOI: 10.1107/s0108767307043930.
- [6] George M. Sheldrick. "SHELXT- Integrated Space-Group and Crystal-Structure Determination". In: Acta Crystallographica Section A Foundations and Advances 71.1 (Jan. 2015), pp. 3–8. ISSN: 2053-2733. DOI: 10.1107/s2053273314026370.
- [7] A. Altomare et al. "Completion and Refinement of Crystal Structures with SIR92". In: Journal of Applied Crystallography 26.3 (June 1993), pp. 343–350. ISSN: 0021-8898. DOI: 10.1107/s0021889892010331.
- [8] Angela Altomare et al. "SIR97: A New Tool for Crystal Structure Determination and Refinement". In: *Journal of Applied Crystallography* 32.1 (Feb. 1999), pp. 115–119. ISSN: 0021-8898. DOI: 10.1107/s0021889898007717.
- [9] George Michael Sheldrick. SHELXL-97, Program for the Refinement of Crystal Structures. 1997.
- [10] George M. Sheldrick. "Crystal Structure Refinement with SHELXL". In: Acta Crystallo-graphica Section C Structural Chemistry 71.1 (Jan. 2015), pp. 3–8. ISSN: 2053-2296. DOI: 10.1107/s2053229614024218.
- [11] D. Waasmaier and A. Kirfel. "New Analytical Scattering-Factor Functions for Free Atoms and Ions". In: *Acta Crystallographica Section A Foundations of Crystallography* 51.3 (May 1995), pp. 416–431. ISSN: 0108-7673. DOI: 10.1107/s0108767394013292.